



## On the natural convective heat transfer from a cold horizontal cylinder over an adiabatic surface

M.H. Sedaghat<sup>1,\*</sup>, M. Yaghoubi<sup>2</sup> and M.J. Maghrebi<sup>3</sup>

<sup>1</sup> Ph.D. Student, Department of Mechanical Engineering, Shahrood University of Technology, Shahrood, Iran

<sup>2</sup> Professor, Department of Mechanical Engineering, Shiraz University, Zand Street, Shiraz, Iran

<sup>3</sup> Associate Professor, Department of Mechanical Engineering, Ferdowsi University of Mashhad, Mashhad, Iran

### Abstract

A steady two-dimensional laminar free convection heat transfer from a cold horizontal isothermal cylinder located above an adiabatic floor is studied both experimentally and numerically. In the experimental measurements the effects of cylinder distance from horizontal floor to its diameter ( $L/D$ ) on heat transfer coefficient is studied for Rayleigh numbers of  $3 \times 10^5$  and  $6 \times 10^5$ . Computations are made using OpenFOAM (an open source) code for wide range of Rayleigh numbers from  $10^4$  to  $10^6$  and comparisons are made with the corresponding experimental measurements. Flow stream lines and isothermal lines are plotted for different cylinder relative positions. Results indicate that cold plume flows downstream and strikes to the horizontal floor and moves horizontally away from cylinder over the horizontal floor. The finite space between cylinder and floor makes the flow different from those cylinders surrounded by an infinite medium. Results also indicate that variation of average heat transfer coefficient of the cold cylinder is highly affected by  $L/D$ . A new correlation for estimation of convection heat transfer for a single horizontal cylinder placed over an adiabatic floor is also developed.

**Keywords:** Free convection; Laminar flow; Cold horizontal cylinder; Adiabatic floor; OpenFOAM.

### 1. Introduction

Applications of free convection from horizontal pipes or tubes carrying cold fluid placed over a floor encounter in many refrigerating equipments, air-conditioning and freezing systems. Studies from a single tube surrounded by infinite fluid have been studied extensively and natural convection heat transfer from horizontal pipes have been the subject of a large number of experimental and theoretical investigations, but there are a few reports for free convection heat transfer to a single cold cylinder over an adiabatic floor.

For a single tube surrounded by an infinite media typical correlation for a wide range of Rayleigh numbers, between  $10^2$  to  $10^7$ , introduced by Morgan [1] as follows:

$$Nu_{\infty} = \begin{cases} 0.85 \times Ra^{0.1818} & 10^2 \leq Ra \leq 10^4 \\ 0.48 \times Ra^{0.25} & 10^4 \leq Ra \leq 10^7 \end{cases} \quad (1)$$

$$\text{where } Nu = \frac{hD}{k} \text{ and } Ra = \frac{g\beta D^3(T_s - T_{\infty})}{\alpha\nu}$$

Kuehn and Goldstein [2] reported a correlation based on numerical studies and compared with experimental measurements. Some related researches are also reported by Tokura et al. [3], Badr [4], Herraes and Belda [5] and Corcione [6].

Effect of adiabatic bounding walls on heat transfer coefficient from a hot circular cylinder is also reported. Saito et al. [7] experimentally studied the effect of a narrow aluminum plate covered by Bakelite plate which is located on the top of a horizontal heated cylinder for Grashof numbers between  $2.1 \times 10^6$  to  $3.2 \times 10^6$ . They showed that the rate of heat transfer would be minimized if the ratio of cylinder space from floor to its diameter ( $L/D$ ) be close to 0.12. They also found that the Nusselt Number is 11% less when there is no floor. Koizumi and Hosokawa [8] used flow visualization to study free convection heat transfer

\* Corresponding author, Phone: (+98) 9178473569, Fax: (+98) 2733335445  
Email: [mh.sedaghat@gmail.com](mailto:mh.sedaghat@gmail.com)

from a pipe under a ceiling. Their experiments include effect of changing pipe diameter, ceiling distance from the pipe and the type of ceiling (adiabatic or isothermal) on natural convection heat transfer for Rayleigh numbers from  $4.8 \times 10^4$  to  $10^7$ . Their results for an isothermal ceiling show that fluid flow almost remains steady and two dimensional for all range of  $L/D$  for the Rayleigh numbers more than  $10^5$ . When the ceiling is close to the pipe ( $L/D=0.4$ ) the fluid flow becomes unstable and three dimensional for Rayleigh number less than  $10^5$ , and also for high values of  $L/D$  the plume oscillate laterally. They also reported variation of local Nusselt number for both types of ceiling at  $Ra=1.3 \times 10^6$  and  $L/D=0.05, 0.2$ . Lawrence et al. [9] studied natural convection heat transfer from a hot pipe below an isothermal surface. They applied finite element method for their numerical solution and Mach-Zehnder interferometer in their experiments for air flow; with Rayleigh numbers of  $10^3$  to  $10^5$  and  $0.1 \leq L/D \leq 0.5$ . They showed that when the distance between ceiling and pipe is larger than the pipe diameter, ceiling does not influence on the rate of heat transfer from the pipe. They also indicated that average Nusselt number increases as a result of conduction heat transfer between the pipe and the ceiling for spacing of about one fourth of cylinder diameter. However, when  $L/D > 0.25$  the ceiling decreases heat transfer up to 10%. Correa et al. [10] studied natural convection from a hot cylinder beneath an adiabatic surface numerically for  $10^2 \leq Ra \leq 10^5$  and  $0.55 \leq L/D \leq 2.5$  using finite volume method. They found that the existence of the surface influences the rate of heat transfer from pipe when  $L/D$  is less than 2 and average Nusselt number is proportional to this ratio. However, their results are different from results of Koizumi and Hosokawa [8] for low values of  $L/D$ . Ashjaee et al. [11] used a Mach-Zehnder interferometer to study natural convection heat transfer from a pipe under an adiabatic ceiling for Rayleigh numbers between  $10^3$  to  $4 \times 10^4$ . They showed that the ceiling did not have a great effect on heat transfer from cylinder when  $L/D > 1.5$ . They also showed that by decreasing the distance to  $L/D=0.5$ , Nusselt number reduced significantly. They reported that by reducing this ratio, and formation of vortex above the cylinder, both local Nusselt number at the top of the cylinder and average Nusselt number decreased sharply. They also suggested a function with two variables of  $L/D$  and Rayleigh number for computing average Nusselt number. Similar investigations are expressed by other authors which focused for heated cylinder being positioned between vertical walls [12-15], below a ceiling [16] or inside a square [17, 18].

Tahavvor and Yaghoubi [19] studied natural convection heat transfer for a cooled horizontal circular cylinder surrounded by an infinite fluid using artificial neural network method for Rayleigh numbers from  $10^6$  to  $10^8$ . They found that local and consequently the average Nusselt number is slightly higher for natural

convection heat transfer from a hot cylinder in free medium when comparing with correlation by Kuehn and Goldstein [2]. For a cold cylinder, the cold plume has the same direction with the gravitational acceleration which leads to a slight increase in Nusselt number. They also suggested a new correlation for natural convection from a cooled horizontal cylinder surrounded in a free space.

According to the literature review, most of the studies are focused on natural convection from hot cylinder and only a few analyses are carried from cooled cylinders or tubes above a floor. Huynh [20] studied the situation of a heated cylinder positioned above a horizontal (isothermal and adiabatic) plane for Rayleigh numbers in the range of  $10^9$ - $10^{11}$ . He used Chien's turbulence model of low-Reynolds-number  $k$ - $\epsilon$  to perform his numerical computations. He showed that the plane's thermal condition (adiabatic or isothermal) in contrast to laminar case has on significant difference in heat transfer rate.

In most refrigeration and freezing systems and components, one can observe pipes which carrying cold refrigerant, located above an adiabatic floor or alongside of a surrounding wall. For such configurations no explicit reports are available.

In this paper, two-dimensional laminar natural convection to a cold horizontal isothermal cylinder above an adiabatic floor is investigated both numerically and experimentally. Experiments are made for various space ratios and Rayleigh numbers and numerical computations are carried for wider range of space ratios and Rayleigh numbers.

## 2. Experimental setup

In Fig. 1 a sketch of the experimental geometry is shown. A horizontal long cylinder placed above an adiabatic floor and surrounded by an ambient air.

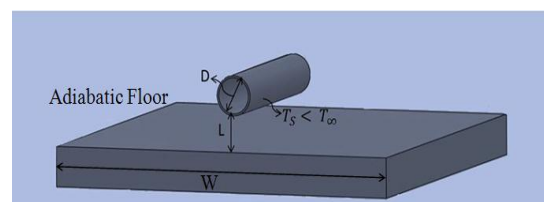


Fig. 1. Cylinder and floor arrangement

In this figure the surface temperature of the cylinder,  $T_s$ , is assumed to be lower than the ambient air temperature,  $T_{\infty}$ , and higher than ambient dew point temperature. The width of floor ( $W$ ) is considered to be sufficiently wide in order to reduce end effects on heat transfer from cylinder. In Fig. 2 the experimental system is shown.

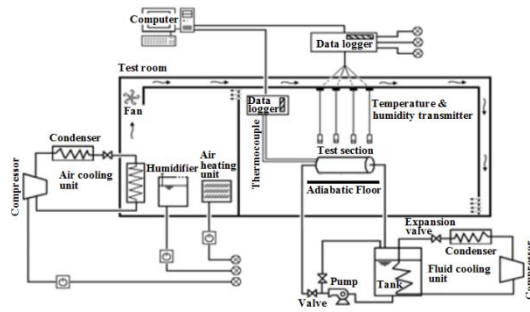


Fig. 2. Experimental system

The main components of the system are: a circular cylinder as a test section (36 cm in length and 8 cm in diameter), adiabatic floor, fluid cooling unit which has R22 as a refrigerant, air cooling unit, air heating unit, humidifier, fan, valves, data logger, T type thermocouples and a computer. This figure shows that temperature of cylinder surface is controlled by a fluid cooling unit which flows in a refrigeration cycle. The T-type thermocouples attached to the cylinder measure temperature at various positions. All of the measured data are recorded by a data logger which is connected to a computer. The test room consists of two blocks; test room and equipment's room which are separated by an isolated wall. In the equipment's room air cooling unit, air heating unit and humidifier control the temperature and humidity of the test room. Fig. 2 also shows that a fan blows air in the space between roof and the suspended ceiling and passes through the holes with reduced air velocity. This velocity at the outlet is less than 0.4 m/s only during fan operation. Free convection condition is maintained in the room for the rest of experimental duration time. More explanation of the system operation is reported by Tahavvor and Yaghoubi [19].

### 2.1. The apparatus and instrumentation

The test section is shown in Fig. 3. This cylinder is made of aluminum which has 36 cm length and 8 cm outside diameter. Sixteen T-type thermocouples are attached to the cylinder to measure its temperature. The thermocouples first calibrated in a controlled water basin with 0.5° C uncertainty. These thermocouples are placed some specific holes with distance of 3 mm from the cold surface. The thermocouples are inserted in the both sides of pipe (eight thermocouples in each side) to measure average heat flux and temperature distribution along the test section. The value of cold surface temperature is determined by averaging the temperature of four thermocouples at each side. As shown in Fig. 3, an insulated layer with the thermal conductivity of 0.17 (W/m.K) is placed between two aluminum layers to obtain high temperature difference and more accurate heat flux.

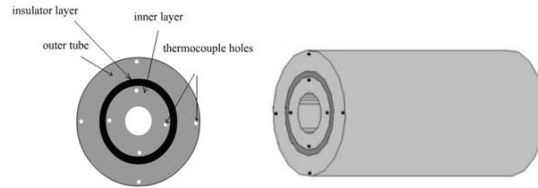


Fig. 3. Test section and thermocouples position

Surface temperature distribution indicates that for steady state condition, heat conduction along the axis of cylinder is negligible in comparison to heat transfer in radial direction. Hence, the axial heat transfer is neglected in this study. Fig. 3 also shows the relative position of thermocouple holes in the insulation layer and outer layer.

Since the thermal conductivity of insulation is much less than the thermal conductivity of aluminum, the thermal resistance of outer layer is negligible in comparison with the thermal resistance of the insulation layer. This leads to a considerable temperature gradient around the insulation which provides an easy way of measuring radial heat flux. The radial heat flux ( $q''$ ), average heat transfer coefficient ( $h_{ave}$ ) and average Nusselt number ( $Nu_{ave}$ ) for experimental measurements are determined by:

$$q'' = \frac{2k_{ins}(T_{out} - T_{in})}{Ln\left(\frac{r_{out}}{r_{in}}\right)D} \quad (2)$$

$$h_{ave} = \frac{q''}{(T_{s,ave} - T_{\infty})} \quad (3)$$

$$Nu_{ave} = \frac{h_{ave}D}{k_f} \quad (4)$$

where  $k_{ins}$  is the thermal conductivity of insulation,  $T_{out}$  and  $T_{in}$  the temperature of outer and inner layer of test section respectively,  $r_{out}$  and  $r_{in}$  the radius of outer and inner layer of test section respectively,  $D$  the diameter of the cylinder,  $T_{s,ave}$  the average temperature of the surface of the cylinder,  $T_{\infty}$  the ambient temperature and  $k_f$  the thermal conductivity of air.

The horizontal adiabatic floor which is placed beneath the test section is made of compact Polystyrene which rated thermal conductivity of 0.029 to 0.045 W/(m K). The surface dimension is 150×100 cm<sup>2</sup> with 4 cm thickness. The insulation is considered to be wide enough to reduce the end effects on heat transfer to the cylinder. Since the flow reaches to steady state condition we assume that the insulated surface temperature is equal to the ambient temperature. So the radiation heat flux can be computed as follow:

$$q''_{rad} = \epsilon_{al} \sigma (T_{\infty}^4 - T_{s,ave}^4) \quad (5)$$

In Eq. (5)  $\sigma$  is the Stefan-Boltzmann constant and has the value of  $5.67 \times 10^{-8}$  W/m<sup>2</sup>.K<sup>4</sup> and  $\epsilon$  is emissivity which for the aluminum surface is 0.09. The worst case

for  $Ra=10^4$  the amount of  $q''_{rad}$  is about  $15 \text{ W/m}^2$  which is negligible compared with free convection heat flux which is in the order of  $745 \text{ W/m}^2$ . In this regard effect of radiation heat transfer is neglected.

The fluid cooling unit is TUV-BERLIN BRANDENBURG. It has the ability to cool the antifreeze solution to  $-30 \text{ }^\circ\text{C}$ . Ethylene-glycol/water of 60/40 solution is used as refrigerant for controlling and keeping the test section surface temperature at a fixed value. Also the cooling unit used is a TUV-BERLIN BRANDENBURG cooling unit. It has the ability to cool the ambient air temperature to  $0 \text{ }^\circ\text{C}$ . The air heating unit consists of three thermal elements, 2000 Watt in power. These elements have the ability to reach the test room air temperature to  $50 \text{ }^\circ\text{C}$ . Two humidifiers are also used to humidify the test room ambient air. These humidifiers have a volume of about 6 liters and have the ability to operate continuously more than 20 hours. According to the volume of the test room these humidifiers are able to reach a relative humidity of the test room to 100% for approximately 4 hours.

The data acquisition units used are ADAM 4518 and 4520MOXA ioLogic respectively. First unit has sixteen analogue input channels, each channel is able to measure, voltage, resistance, current or frequency. It is used to measure the thermocouple outputs. Second unit is used to measure relative humidity and temperature of air in the test room. According to these data, command signals are relative humidity and temperature of the ambient air of the test room. These values are measured using four TMH-1 transmitters. These transmitters provide a reliable and economical method for most relative humidity and temperature monitoring applications. Each unit is factory calibrated to provide excellent sensitivity, fast response and stability. The unit features a simple installation with a direct USB connection. Free friendly user software converts the signals into both a humidity and temperature meter.

## 2.2. Experimental procedure and measurements

The experimental setup is shown in Fig. 4. For experimental measurements, ambient air temperature has been maintained at a uniform temperature at  $T_\infty=30\pm 0.2 \text{ }^\circ\text{C}$  and relative humidity of  $30\pm 0.5$  percent.

Experiments are performed for two surface temperatures of  $T_s=13\pm 0.1 \text{ }^\circ\text{C}$  and  $T_s=21\pm 0.1 \text{ }^\circ\text{C}$  which are well above the dew point of air temperature. In these conditions, Rayleigh numbers based on the cylinder diameter are  $6\times 10^5$  and  $3\times 10^5$ , respectively. The experiments are performed for  $L/D=0.1, 0.3, 0.5, 0.75, 1$  and  $1.5$  with aforementioned Rayleigh numbers. During each experiment cylinder ends are insulated with a thin polyethylene film so that heat transfers occur only in the radial direction.

After the surface temperature reached to the desired temperature, and becomes steady which takes about

two hours, measurements started. Each test is started by saving the temperature of all thermocouples in a data logger connected to a PC computer. Based on the recorded average temperature, radial heat flux is calculated by Eq. (2).

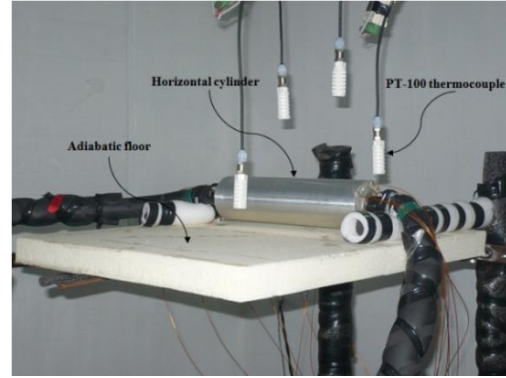


Fig. 4. Experimental arrangement of cylinder on adiabatic floor

## 3. Numerical method

### 3.1. Computational modeling

Physical model for CFD solution is shown in Fig. 5. The flow is symmetrical about a vertical plane passing through the axis of the cylinder. Thus, the solution domain is bounded by a half-cylinder surface, the two lines of symmetry and surface floor. The outer boundary has a pressure outlet boundary condition with ambient temperature ( $T_\infty$ ) and zero gradient pressure.

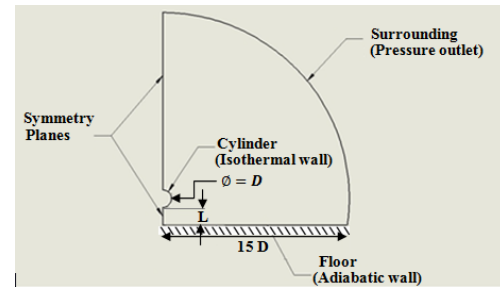


Fig. 5. Physical geometry and computational domain

The governing equations for two-dimensional, laminar, natural convection around a horizontal cylinder with Boussinesq approximation consist of continuity, momentum and energy equations:

$$\frac{\partial u}{\partial x} + \frac{\partial v}{\partial y} = 0 \quad (6)$$

$$\rho(u \frac{\partial u}{\partial x} + v \frac{\partial u}{\partial y}) = -\frac{\partial P}{\partial x} + \mu(\frac{\partial^2 u}{\partial x^2} + \frac{\partial^2 u}{\partial y^2}) \quad (7)$$

$$\rho(u \frac{\partial v}{\partial x} + v \frac{\partial v}{\partial y}) = -\frac{\partial P}{\partial y} + \mu(\frac{\partial^2 v}{\partial x^2} + \frac{\partial^2 v}{\partial y^2}) + \rho g \beta (T - T_\infty) \quad (8)$$

And

$$\rho C(u \frac{\partial T}{\partial x} + v \frac{\partial T}{\partial y}) = k(\frac{\partial^2 T}{\partial x^2} + \frac{\partial^2 T}{\partial y^2}) \quad (9)$$

The corresponding boundary conditions are prescribed in Table 1 and the non-dimensional parameters related to the governing equations are defined as follows:

$$Ra = \frac{g\beta D^3(T_s - T_\infty)}{\alpha\nu} \quad Nu = \frac{hD}{K_f} \quad \eta = \frac{L}{D} \quad (10)$$

where  $g$  is the gravitational acceleration,  $\beta$  the volumetric expansion coefficient,  $T_s$  the temperature of the cylinder surface,  $\alpha$  the thermal diffusivity,  $\nu$  the kinematic viscosity,  $h$  the convection heat transfer coefficient and  $K_f$  the fluid conductivity.

The governing equations are solved using OpenFOAM, an open-source CFD code. The OpenFOAM is an enormously powerful research CFD code, written in the programming language C++. OpenFOAM uses finite volume scheme to solve systems of partial differential equations ascribed on any 3D unstructured mesh of polyhedral cells. The fluid flow solvers are developed within a robust, implicit, pressure-velocity, iterative solution framework, although alternative techniques are applied to other continuum mechanics solvers. Domain decomposition parallelism is fundamental to the design of OpenFOAM and integrated at a low level so that solvers can generally be developed without the need for any 'parallel-specific' coding. In this study the incompressible Navier Stokes equations are solved by using the PISO algorithm.

The pre-processing open-source software Gambit is used to create the grids of the computational model. The computational domain is taken very far to resemble ambient domain. Fig. 6 shows the generated grid for the numerical solution.

**Table 1. Boundary conditions for the domain of Fig. 5**

	T(K°)	U(m/s)	P(pa)
<b>Surrounding</b>	Fixed value	Pressure outlet	Fixed value
<b>Floor</b>	Zero gradient	Fixed value	Zero gradient
<b>Symmetry planes</b>	symmetry	symmetry	symmetry
<b>Cylinder</b>	Fixed value	Fixed value	Zero gradient

### 3.2. Numerical computations

Numerical modeling is done for  $L/D=0.1, 0.3, 0.5, 1$  and  $1.5$  and Rayleigh numbers ranging from  $10^4$  to  $10^6$  which correspond to different values of the cylinder diameter ( $D$ ), cylinder temperature ( $T_s$ ) and the

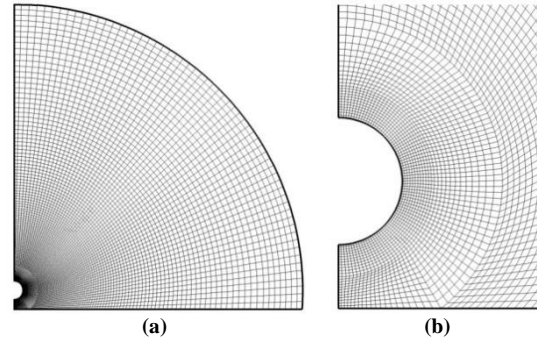


**Fig. 6. Generated grid for numerical solution (a) whole domain and (b) near the cylinder**

ambient temperature ( $T_\infty$ ). Table 2 shows the specifications of various cases considered for the simulation. From energy balance at the cylinder surface, following expressions for the local and average Nusselt number from numerical computations are obtained.

### 3.2. Numerical computations

Numerical modeling is done for  $L/D=0.1, 0.3, 0.5, 1$  and  $1.5$  and Rayleigh numbers ranging from  $10^4$  to  $10^6$  which correspond to different values of the cylinder diameter ( $D$ ), cylinder temperature ( $T_s$ ) and the ambient temperature ( $T_\infty$ ). Table 2 shows the specifications of various cases considered for the simulation. From energy balance at the cylinder surface, following expressions for the local and average Nusselt number from numerical computations are obtained.

$$q'' = k_f \frac{\partial T}{\partial r} \Big|_{r=D/2} \quad (11)$$

$$h_\theta = \frac{q''}{(T_s - T_\infty)} \quad (12)$$

$$h_{ave} = \frac{1}{\pi} \int_0^\pi h_\theta d\theta \quad (13)$$

$$Nu_\theta = \frac{h_\theta D}{k_f} \quad (14)$$

$$Nu_{ave} = \frac{h_{ave} D}{k_f} \quad (15)$$

**Table 2. Various cases of numerical computations**

Ra	D (m)	T <sub>s</sub> (C°)	T <sub>∞</sub> (C°)
10 <sup>4</sup>	0.016	13	41.5
10 <sup>5</sup>	0.04	13	29.5
3×10 <sup>5</sup>	0.08	21.5	31.5
6×10 <sup>5</sup>	0.08	13	31.5
10 <sup>6</sup>	0.08	13	32.5

#### 4. Results and discussion

At this section, the validity the CFD solver and grid dependency of the solution method will be explained.

To obtain a grid independent solution, various meshes are considered. Figure 7-a shows the average Nusselt number obtained for different meshes for a cylinder in an infinite media for  $Ra=10^6$ . According to this figure, the average Nusselt number almost becomes stable for mesh sizes larger than 7500. Figure 7-b also shows the variation of average Nusselt number according to the ratio of numerical domain to pipe diameter ( $R/D$ ) for a cylinder in an infinite media for a  $Ra=10^6$ . This figure also illustrates that the value of average Nusselt number become constant after  $R/D=15$  which means that the solution is domain-independent.

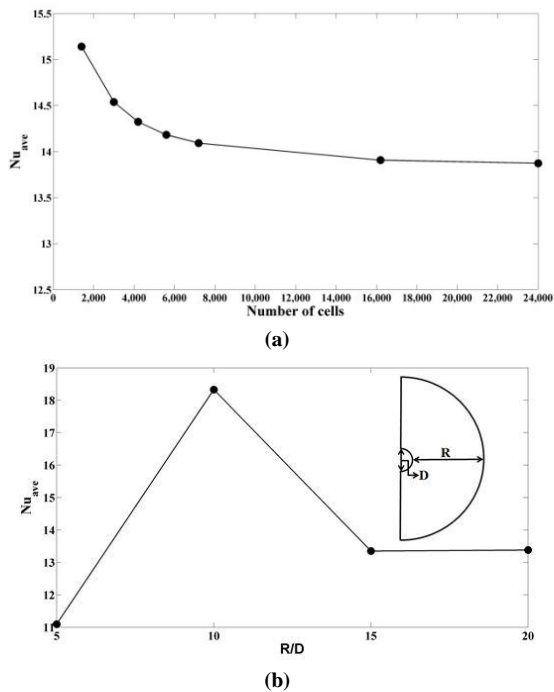


Fig. 7. Solution Independency based on average Nusselt number (a) Grid independency and (b) domain independency

To validate the present CFD solver, numerical results with experimental measurements are compared for two Rayleigh numbers  $3 \times 10^5$  and  $6 \times 10^5$ . For experimental measurements  $Nu_{ave}$  and  $Nu_{\infty}$  are determined from Eq. (4) and for numerical computations they are calculated from Eq. (13). Good agreements are observed between experimental measurements and numerical computations. Maximum difference between the experimental measurements and numerical results is about 6 percent in Fig.8.

The OpenFOAM code solves the equation unsteadily and for the present study computations are

continued to reach a steady condition. For a typical calculation for a pipe in an infinite media and for  $Ra=10^4$ , after 100 seconds the velocity residual becomes less than  $10^{-6}$  and the temperature residual reduces more than  $10^{-5}$ .

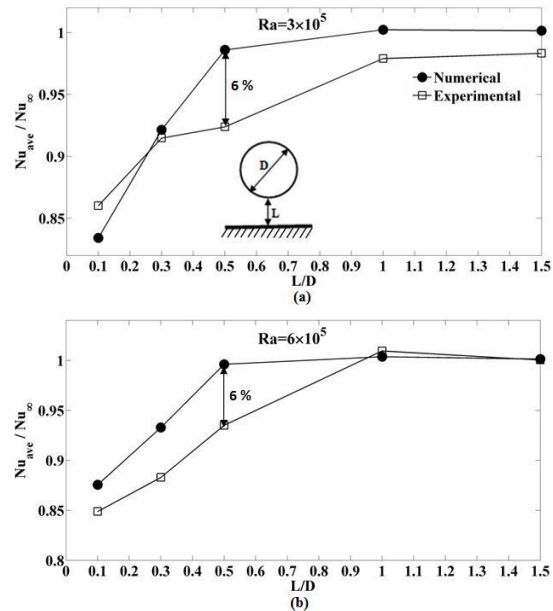


Fig. 8. Comparison of  $Nu_{ave}/Nu_{\infty}$  for numerical and experimental measurements as a function of  $L/D$  for (a)  $Ra=3 \times 10^5$  and (b)  $Ra=6 \times 10^5$

Based on the valid code, details of more numerical computations for flow field and temperature field are computed. Figure 9 indicates the streamlines around a half of the cylinder for different Rayleigh numbers;  $Ra=10^4$ ,  $Ra=10^5$  and  $Ra=10^6$ . This figure shows that the flow moves away about at an angle of  $120^\circ$  from the surface of the cylinder and this angle is increased by addition of  $L/D$  for  $Ra=10^4$ . For a specific value of  $L/D$  this angle raises by any increase in Rayleigh number which results from the thinning boundary layer. This means that the influence of adiabatic floor on the flow reduces as either  $L/D$  or Rayleigh number increases. This figure also illustrates that for  $Ra=10^4$  even for  $L/D=1.5$  the flow differs from the streamlines around a cylinder without a floor ( $L/D=\infty$ ). By increasing Rayleigh number the effects of flow disappear at lower amount of  $L/D$ ; for example for  $Ra=10^6$  the flow pattern becomes similar around the cylinder when  $L/D \geq 1$  and it resembles the flow pattern for a cylinder in an infinite media ( $L/D=\infty$ ).

Fig. 10 indicates isothermal lines around the horizontal cylinder for various  $L/D$  and for  $Ra=10^4$  and  $Ra=10^6$ . It represents that the cold plume flows downstream strikes to the floor and moves horizontally away from the cylinder over the floor. The finite space between the cylinder and the floor makes

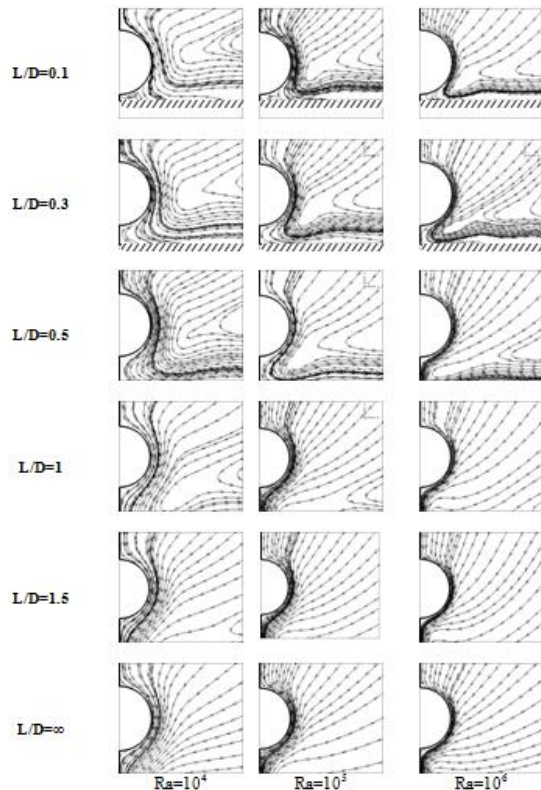


Fig. 9. Streamlines around cylinder for various L/D and Rayleigh numbers

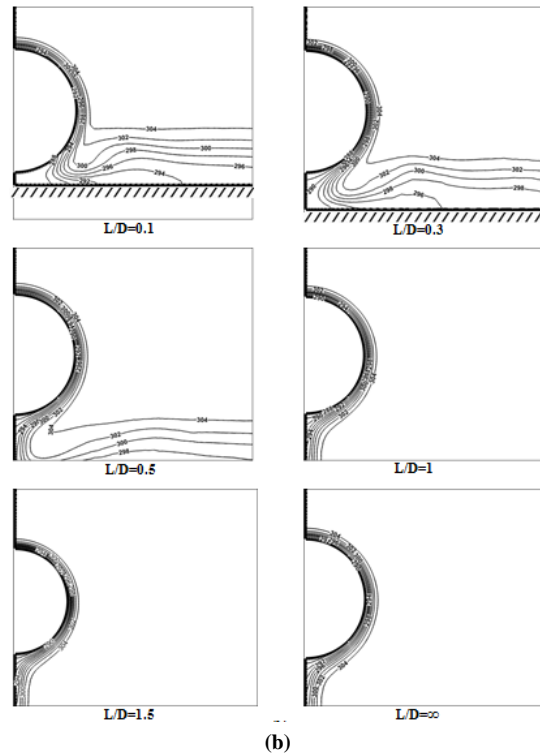
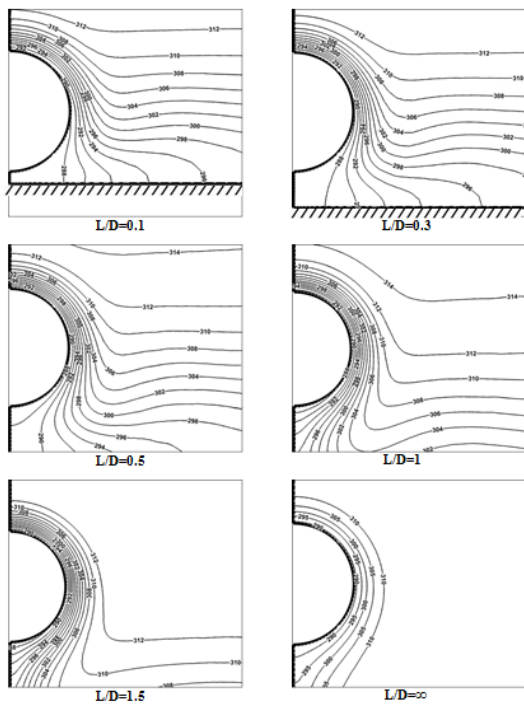


Fig. 10. Isothermal lines around the cylinder for various L/D for (a)  $Ra=10^4$  and (b)  $Ra=10^6$



(a)

the flow pattern different from cylinders located in an infinite media. These figures also illustrate that by increasing the amount of L/D for each Rayleigh number, the thermal boundary layer becomes thinner which results reduction of the influence of adiabatic floor and consequently corresponding Nusselt number increases.

Fig. 11 indicates variation of local Nusselt number around the cylinder as a function of radial angle  $\theta$  for various L/D. Fig. 11-a shows that the adiabatic floor has a significant influence on the local Nusselt number and this effect decreases the value of  $Nu_\theta$  even at  $\theta=0$ .

But as indicated in Fig. 11-b, this effect is reduced by increasing the Rayleigh number. The effect of adiabatic floor on local Nusselt number starts around  $\theta=40^\circ$ .

This means that boundary layer becomes aware of the adiabatic floor at higher angles of  $\theta$  by increasing Rayleigh number. In addition, for a specific L/D the differences of local Nusselt number between the confined cylinder and a cylinder in a free space ( $L/D=\infty$ ) rises by increasing  $\theta$ . This means that adiabatic floor affects the flow in proportion to the angles from top of the cylinder.

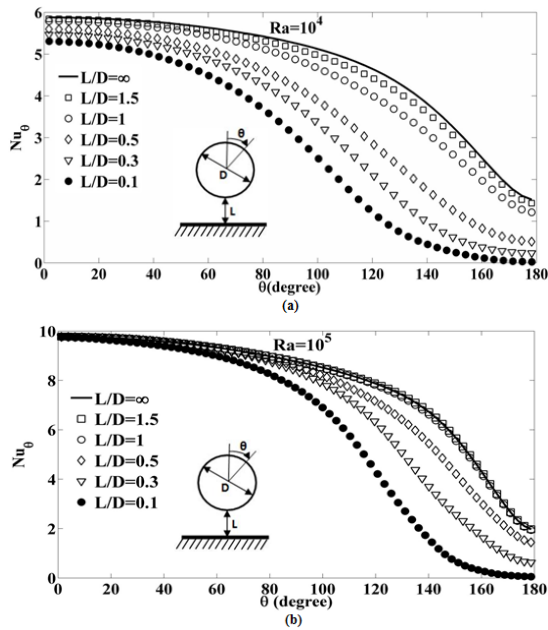


Fig. 11. Variation of local Nusselt number around cylinder for (a)  $Ra=10^4$  and (b)  $Ra=10^5$

Figure 12 illustrates variation of average Nusselt number as a function of  $L/D$  for different Rayleigh numbers. This figure indicates that at a fixed value of  $L/D$  by increasing Rayleigh number, the ratio of  $Nu_{ave}/Nu_{\infty}$  grows. For example this figure shows that the value of  $Nu_{ave}/Nu_{\infty}$  is about 0.6 for  $Ra=10^4$  and  $L/D=0.1$  and this ratio increases by increasing the Rayleigh number. This ratio reaches approximately to 0.92 for  $Ra=10^6$ . By increasing Rayleigh number for lower value of  $L/D$  the ratio of  $Nu_{ave}/Nu_{\infty}$  approaches to 1. For example the average Nusselt number for  $L/D=1.5$  and  $Ra=10^4$  is not equal to the average Nusselt number of a cylinder surrounded by an infinite fluid. However, for  $Ra=10^6$  the average Nusselt number is equal to the Nusselt number of the cylinder with any surrounding wall at  $L/D=0.5$ . These effects may be due to the thinning of thermal boundary layer around the cylinder for higher Rayleigh numbers. This means that Rayleigh number should be regarded as one of the significant factors which influence the ratio of  $Nu_{ave}/Nu_{\infty}$  on the cylinder. On the other hand, for a fixed Rayleigh number (especially for low Rayleigh numbers),  $L/D$  has a great effect on the heat transfer ratio. For instance for  $Ra=10^4$  and in  $L/D=0.1$ , the value of average Nusselt number around the cylinder is almost 60% of the average Nusselt number of the cylinder without adiabatic floor. Thus both  $L/D$  and Rayleigh number can influence free convection heat transfer from a cold horizontal cylinder.

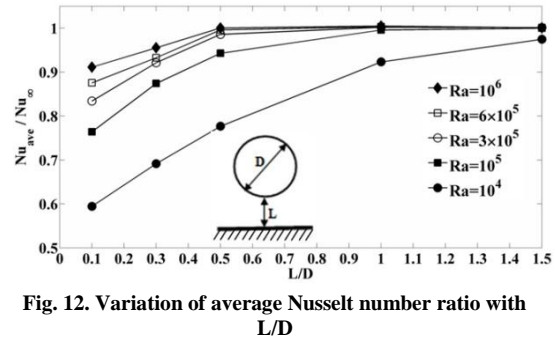


Fig. 12. Variation of average Nusselt number ratio with  $L/D$

From numerical computations a new relation for  $Nu_{ave}/Nu_{\infty}$  as a function of Rayleigh number and  $\eta=L/D$  is obtained as:

$$\frac{Nu_{ave}}{Nu_{\infty}} = A + \frac{B}{Ra} + \frac{C}{Ra^2} + D\eta + E\eta^2 + F \frac{\eta}{Ra} \quad (16)$$

with  $R^2 = 0.958$

$$\text{for } \begin{cases} 0 \leq \eta \leq 1.5 \\ 10^4 \leq Ra \leq 10^6 \end{cases}$$

where

$$\eta = \frac{L}{D}, \quad Ra = \frac{g \beta D^3 (T_s - T_{\infty})}{\alpha \nu}$$

And

$$A = 0.851, \quad B = -7890.315, \quad C = 47939464.631, \quad D = 0.363 \\ E = -0.171, \quad F = 1860.061$$

The value of  $Nu_{\infty}$  is obtained from Eq. (1) for a cylinder surrounded by a free space.

## 5. Uncertainty

Analysis of uncertainty is required in order to evaluate the accuracy of measurements which is similar to the one described in the work of Batista et al. [21]. For any quantity  $M$ , the total uncertainty  $U$  can be determined from uncertainties of specified components which influence the experiment [22]. For the parameter  $M$ , whose results depend on uncorrelated input estimates  $x_1, x_2, \dots, x_n$ , the standard uncertainty of the measurement is obtained by appropriately combining the standard uncertainties of these input estimates. The combined standard uncertainty of the estimate  $M$  denoted by  $U$  is calculated from the following equations [23].

$$M = f(x_1, x_2, \dots, x_n) \quad (17)$$

$$U^2(M) = \sum_{i=1}^n \left[ \frac{\partial f}{\partial x_i} \right]^2 U^2(x_i) \quad (18)$$

where  $f$  is the function of  $M$  in terms of input, estimates  $x_1, x_2, \dots, x_n$ , and each  $U(x_i)$  is a standard uncertainty of any input.

The expression for the standard uncertainty associated with  $h_{ave}$  is developed from Eq. (2) and Eq. (3), using the law of propagation of uncertainty. The resulting expression is:

$$\begin{aligned} \delta h_{ave} = & \left[ \left( \frac{\partial h_{ave}}{\partial T_{\infty}} \delta T_{\infty} \right)^2 + \left( \frac{\partial h_{ave}}{\partial T_{out}} \delta T_{out} \right)^2 \right. \\ & + \left( \frac{\partial h_{ave}}{\partial T_{in}} \delta T_{in} \right)^2 + \left( \frac{\partial h_{ave}}{\partial D} \delta D \right)^2 \\ & \left. + \left( \frac{\partial h_{ave}}{\partial r_{out}} \delta r_{out} \right)^2 + \left( \frac{\partial h_{ave}}{\partial r_{in}} \delta r_{in} \right)^2 \right]^{\frac{1}{2}} \end{aligned} \quad (19)$$

So

$$\begin{aligned} \delta h_{ave} = & \frac{1}{(T_{ave} - T_{\infty})^2} \left[ \left( \frac{1}{(T_{ave} - T_{\infty})} \frac{2k_{ins}(T_{out} - T_{in})}{D \ln\left(\frac{r_{out}}{r_{in}}\right)} \delta T_{\infty} \right)^2 \right. \\ & + \left( \frac{2k_{ins}}{D \ln\left(\frac{r_{out}}{r_{in}}\right)} \delta T_{out} \right)^2 + \left( \frac{-2k_{ins}}{D \ln\left(\frac{r_{out}}{r_{in}}\right)} \delta T_{in} \right)^2 \\ & + \left( \frac{-2k_{ins}(T_{out} - T_{in})}{D^2 \ln\left(\frac{r_{out}}{r_{in}}\right)} \delta D \right)^2 + \left( \frac{-2k_{ins}(T_{out} - T_{in})}{r_{out} D \left( \ln\left(\frac{r_{out}}{r_{in}}\right) \right)^2} \delta r_{out} \right)^2 \\ & \left. + \left( \frac{2k_{ins}(T_{out} - T_{in})}{r_{in} D \left( \ln\left(\frac{r_{out}}{r_{in}}\right) \right)^2} \delta r_{in} \right)^2 \right]^{\frac{1}{2}} \end{aligned} \quad (20)$$

Lists of the experimental values for different parameters and associated uncertainties for  $Ra=6 \times 10^5$  and  $L/D=\infty$  are prescribed in Table 3. The maximum uncertainty of the measurements is determined according to Table 3 and it is about 20%.

**Table 3. Values for the parameters of Eq. (18)**

parameter	$x_i$	$\delta x_i$	$\frac{\partial h_{ave}}{\partial x_i} \delta x_i$
$T_{\infty}$ (C°)	31.5	0.2	0.0463
$T_{out}$ (C°)	13	0.1	0.1408
$T_{in}$ (C°)	9.96	0.1	-0.1408
$D$ (mm)	80	0.02	-0.0011
$r_{out}$ (mm)	25.9	0.02	-0.0202
$r_{in}$ (mm)	22	0.02	0.0238

## 6. Conclusion

The influence of an adiabatic floor on natural convection heat transfer from a cold horizontal cylinder is studied both numerically and experimentally. Results indicate that:

1. The value of Rayleigh number and the ratio of cylinder spacing from adiabatic floor ( $L/D$ ) are two important factors which have great influence on heat transfer from the horizontal cylinder.
2. For higher Rayleigh numbers, variation of local Nusselt number over the cylinder starts latter for higher angle  $\theta$  as a result of thinner thermal boundary layer. For example the variation of local Nusselt number for  $Ra=104$  starts even at the angle of 0 but by increasing Rayleigh number to  $Ra=10^5$  this variation starts about at an angle of 70°.
3. By increasing Rayleigh number, the ratio of  $Nu_{ave}/Nu_{\infty}$  increases for a fixed value of  $L/D$ . The heat transfer ratio approaches to 1 for lower values of  $L/D$ , e.g. for  $Ra=10^4$  the value of  $Nu_{ave}/Nu_{\infty}$  does not reach to 1 even for  $L/D=1.5$  but for higher values of  $Ra=3 \times 10^5$  this ratio reaches to 1 for  $L/D=0.5$ . This means that by increasing Rayleigh number the effect of adiabatic floor on natural convection from the cylinder, is reduced. Heat transfer ratio increases more sharply for a fixed value of Rayleigh number (in particular for low Rayleigh numbers) by increasing  $L/D$ .

For practical applications a new correlation developed which can estimate the ratio of  $Nu_{ave}/Nu_{\infty}$  as a function of Rayleigh number and  $L/D$ .

## References

- [1] Morgan VT (1975) The overall convective heat transfer from smooth circular cylinders. *Advances in Heat Transfer* 11: 199–264.
- [2] Kuehn TH, Goldstein RJ (1980) Numerical solution to the Navier-Stokes equations for laminar natural convection about a horizontal isothermal circular cylinder. *Int J Heat Mass Tran* 23: 971–979.
- [3] Tokura H, Saito K, Kisinami K, Muramoto M (1983) An experimental study of free convection heat transfer from a horizontal cylinder in a vertical array set in free space between parallel walls. *J Heat Trans-T ASME* 105:102–107.
- [4] Badr HM (1987) Heat transfer in transient buoyancy driven flow adjacent to a horizontal rod. *Int J Heat Mass Tran* 30: 1997–2012.
- [5] Herraes JV, Belda RA (2002) Study of free convection in air around horizontal cylinders of different diameter based on holographic interferometry. *Int J Therm Sci* 41: 261–267.

- [6] Corcione MC (2005) Correlating equations for free convection heat transfer from horizontal isothermal cylinders set in a vertical array. *Int J Heat Mass Tran* 48: 3660–3673.
- [7] Saito T, Ishiguro R, Fujishima Y (1969) Natural convection heat transfer around a horizontal cylinder (effect of a horizontal plate placed above the cylinder). *Proceeding of the 6<sup>th</sup> National Heat Transfer Symposium of Japan*: 61–64.
- [8] Koizumi H, Hosokawa I (1996) Chaotic behavior and heat transfer performance of natural convection around a hot horizontal cylinder affected by a flat ceiling. *Int J Heat Mass Trans* 39: 1081–1091.
- [9] Lawrence GB, Jardine GE, Naylor D, Machin AD (1999) Free convection from a horizontal heated cylinder located below a ceiling. *Transaction of the CSME* 23:19–35.
- [10] Correa M, Parra R, Vidal A, Rodriguez J, Aguilera ME, Gonzalez D (2005) Natural convection around a horizontal cylinder near an adiabatic cover wall. *Proceeding of Fourth ICCHMT Paris, France* 336.
- [11] Ashjaee M, Eshtiaghi AH, Yaghoubi M, Yousefi T (2007) Experimental investigation on free convection from a horizontal cylinder beneath an adiabatic ceiling. *Exp Therm Fluid Sci* 32:614–623.
- [12] Farouk B, Guceri SI (1982) Natural and mixed convection heat transfer around a horizontal cylinder within confining walls. *Numer Heat Tr* 5: 329–341.
- [13] Karim F, Farouk B, Namer I (1986) Natural convection heat transfer from a horizontal cylinder between vertical confining adiabatic walls. *J Heat Tarns* 108: 291–298.
- [14] Ma L, van der Zanden J, van der Kooi J, Nieuwstadt FTM (1994) Natural convection around a horizontal cylinder in infinite space and within confining plates: A finite element solution. *Numer Heat Transfer part A Appl* 25: 441–456.
- [15] Sadeghipour MS, Razi YP (2001) Natural convection from a confined horizontal cylinder: the optimum distance between the confining walls. *Int J Heat Mass Trans* 44: 367–374.
- [16] Atmane MA, Chan VSS, Murray DB (2003) Natural convection around a horizontal heated cylinder. *Int J Heat Mass Tran* 46: 3661–3672.
- [17] Sheikholeslami M, Gorji-Bandpay M, Ganji DD (2012) Magnetic field effects on natural convection around a horizontal circular cylinder inside a square enclosure filled with nanofluid. *Int Commun Heat Mass* 39: 978–986.
- [18] Bararnia H, Soleimani S, Ganji DD, (2011) Lattice Boltzmann simulation of natural convection around a horizontal elliptic cylinder inside a square enclosure. *Int Commun Heat Mass Transf* 38: 1436–1442.
- [19] Tahavvor AR, Yaghoubi M (2008) Natural cooling of horizontal cylinder using Artificial Neural Network (ANN). *Int Commun Heat Mass Transf* 35: 1196–1203.
- [20] Huynh BP (2007) Cooling by free convection at high Rayleigh number of cylinders positioned above a plane, 16th Australasian Fluid Mechanics Conference, Crown Plaza, Gold Coast, Australia .
- [21] Batista E, Pinto L, Filipe E, Van der Veen AMH (2007) Calibration of micropipettes: Test methods and uncertainty analysis. *Measurement* 40: 338–342.
- [22] Teoch PL, Shirinzadeh B, Foong CW, Alici G (2002) The measurement uncertainties in the laser Interferometry-based sensing and tracking technique. *Measurement* 32: 135–150.
- [23] Wang X, Bibeau E, Naterer GF (2007) Experimental correlation of force convection heat transfer from a NACA air foil. *Exp Therm Fluid Sci.* 31: 1073–1084.
- [24] Wang CC, Huang RT, Sheu WJ, Chang YJ (2004) Some observation of the formation in free convection: with and without the presence of electric field. *Int J Heat Mass Trans* 47: 3491–3505.